JOURNAL OF AIRCRAFT
Vol. 46, No. 5, September–October 2009

Unmanned Air Vehicle Wing-Tip Corona Nonlinear Effect on Atmospheric Electric Field Measurements

Xingya Da,* Huairong Shen,† Lei Hong,‡ and Rui Zhang§
Academy of Equipment Command & Technology, 101416 Beijing, People's Republic of China

DOI: 10.2514/1.42575

The use of aircraft to measure the electric field in clouds has been ongoing for several decades to study electrification mechanisms of clouds. However, the measurements have been problematic partially due to corona emissions at sharp metallic points. The demand for reliable, robust, and precise measurements requires the study of the corona effect in theory rather than based on uncertain measurements. By using numeric studies of the TF-1 unmanned air vehicle employing four electric field mills, problems caused by wing-tip corona emissions are presented in this paper. The wing-tip corona current model, of net charge Q, field component E_y, and wind speed w, is established based on a space-charge-limited method. Numerical results indicate wing-tip corona effects are nonlinear and are proportional to E_zQ and E_zE_y. Field component E_x is more problematic to retrieve than other field components whether or not the field mills are located downstream of the plume when corona ions are present. To improve measurement precision, it is necessary to consider the nonlinear corona effect and detect definitely when and where corona ions are emitted, especially for manned aircraft.

I. Introduction

MEASUREMENTS of atmospheric electric fields in clouds and storms greatly contribute to the differentiation between those electrification mechanisms advocated in the last few decades or more. However, the mechanisms whereby clouds become electrified and lightning is produced are not satisfactorily understood. To solve this problem, aircraft have been widely applied in measuring fields in clouds and storms, such as the T-28 of the South Dakota School of Mines and Technology [1]; the Special Purpose Test Vehicle for Atmospheric Research of the New Mexico Institute of Mining and Technology [2,3]; and the Altus [4], Lear 28/29 [5–7], and others of NASA in the past few decades. Using aircraft to measure electric fields is theoretically simple; however, obtaining reliable and robust electric field measurements is rather complex due to the difficulty in designing and calibrating field mills, as well as the difficulty in determining the effects caused by corona emissions and so on. The latest field mill designed by the NASA Marshall Space Flight Center and the University of Alabama in Huntsville currently has excellent performance exhibiting high sensitivity, wide dynamic and measurement ranges, and very low noise [8]. Field mill calibration, the core of aircraft electric field measurements, is an intricate process; it is difficult to acquire robust and convergent input–output relations, namely, the relations between the ambient field, net charge, and the mills' outputs. In the 1990s, many effective methods were proposed [5,9]. Koshak's latest calibration method [6] can retrieve storm fields within an error of 12% in simulations [7] and takes into consideration the errors in the field measurement and the mean fair-weather field function. Another method proposed by Mach and Koshak [10] can converge after a few iterations. These improvements make the measurements more reliable and robust.

In contrast, problems caused by corona emissions are difficult to determine by directly analyzing aircraft field measurements [1–3]. Information about the place and time that corona ions were emitted, as well as the magnitude of the corona current, is essential to determine the corona effects. Unfortunately, using aircraft field measurements in these corona-predicting and corona-calculating processes is not an easy (and is perhaps an impossible) task. How corona emissions affect field measurements is still a question to be answered.

Currently, attempts are underway to apply the TF-1 unmanned air vehicle (UAV) to the measurement of atmospheric electric fields. The TF-1 is China's first-generation aeroexploration UAV, designed to measure meteorological data such as wind speed, temperature, pressure, and humidity. Additional information on the evolving charge structure of electrified clouds can be obtained if the TF-1 is used to measure the field. Yet, before taking a flight test, it is necessary to understand the corona effects. Rather than a measurement-based study, we have chosen to conduct a theoretical study, motivated by the physics that corona discharge is determined by the electric field distribution around the corona point. In this paper, we will present our theoretical study on the corona effects at the wing tip, where corona emission is most likely to take place. The road map for this paper can be found in Fig. 1, which itemizes the general ideas of the theoretical study. Because the field distribution around the wing tip is essential to calculating the wing-tip corona current, the first key task is the computation of the electric field for the aircraft, as seen in box A. Furthermore, the tasks in boxes A and B have been completed in previous works [11–13]. Therefore, we will not pursue the details of those two boxes in this paper, but only briefly introduce the methods that were used. Details of boxes C, D, and E will be presented.

II. Field Computational Method for Aircraft

Because the corona discharge is determined by the field distribution around a corona point, the first task is to compute the electric field distribution around the wing tip, namely, the process in box A of Fig. 1. The field computational method for aircraft used in this paper establishes the computational model of the electric field, which can be expressed as

$$\boldsymbol{E} = \boldsymbol{C}[E_x \quad E_y \quad E_z \quad Q]^T \tag{1}$$

where $\boldsymbol{C}$ is a 3×4 matrix called the electric field enhancement factor; E_x, E_y, and E_z are the field components in the aircraft body frame (see Fig. 3); and Q is the net charge on the surface. The numerical computational method for $\boldsymbol{C}$ is based on the method of moments. At the core of the computational method for $\boldsymbol{C}$ is the use of symmetrical surface meshing and the solution of the systems of electric potential equations based on eigenvalue decomposition. These

Received 5 December 2008; revision received 10 March 2009; accepted for publication 11 March 2009.

*Postgraduate, Postgraduate College; Dxingya@gmail.com.
†Professor, Department of Aeronautics; Shenhuair@tom.com.
‡Postgraduate, Postgraduate College; Redleilei@163.com.
§Teaching Assistant, Key Laboratory; Mary1984@126.com.

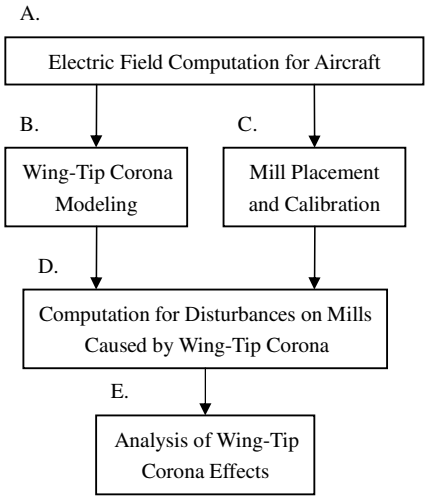

Fig. 1 General ideas for the analysis of wing-tip corona effects.

special techniques could guarantee computation speed and precision. As the derivation of this method is lengthy, more details can be found in [11,12].

The three-dimensional model of the TF-1 can be found in Fig. 3. The electric field computational results for the two wing tips of the TF-1 are

$$\boldsymbol{E}_{\text{left tip}} = \begin{bmatrix} -1.08 & -193.54 & 0.24 & -107.31/4\pi\varepsilon_0 \\ 5.74 & 601.46 & -0.78 & 333.23/4\pi\varepsilon_0 \\ 0.01 & 1.40 & 0.96 & 0.76/4\pi\varepsilon_0 \end{bmatrix} \begin{bmatrix} E_x \\ E_y \\ E_z \\ Q \end{bmatrix} \tag{2}$$

$$\boldsymbol{E}_{\text{right tip}} = \begin{bmatrix} -1.08 & -193.54 & 0.24 & 107.31/4\pi\varepsilon_0 \\ 5.74 & 601.46 & -0.78 & -333.23/4\pi\varepsilon_0 \\ 0.01 & 1.40 & 0.96 & -0.76/4\pi\varepsilon_0 \end{bmatrix} \begin{bmatrix} E_x \\ E_y \\ E_z \\ Q \end{bmatrix} \tag{3}$$

where ε_0 is the vacuum permittivity, and the measurement units of electric field and aircraft net charge are quantified in volts per meter and coulombs, respectively.

III. Wing-Tip Corona Model

Our reason for first studying the wing-tip corona effects is that the field computational results of the TF-1 show that corona emissions are most likely to take place at the wing tips. A wing-tip corona current has been modeled in a previous work [13], based on the idea of the space-charge-limited method [14]. The space-charge-limited method, derived from Poisson's equation for electrostatics, is frequently used for quantitative studies and agrees well with experiments by proposing suitable plasma transition regions. We proposed a semispherical plasma transition region for wing-tip corona discharge with its outer radius determined by wind speed; see the semisphere in Fig. 2.

The field distribution in the semisphere was calculated by the same method used in Sec. II. The fitted results of the electric field in the left and right wing semispheres are

$$E(r,\text{left}) = \frac{1}{r+0.000277}\left(\frac{0.0921Q}{4\pi\varepsilon_0} + 0.1621E_y\right) \tag{4}$$

$$E(r,\text{right}) = \frac{1}{r+0.000277}\left(-\frac{0.0921Q}{4\pi\varepsilon_0} + 0.1621E_y\right) \tag{5}$$

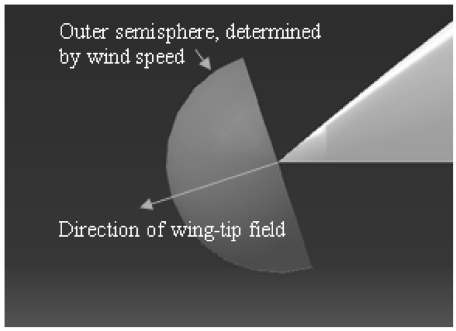

Fig. 2 Proposed semispherical plasma transition region.

Here, r (in meters) is the radius relative to the wing tip, and the measurement units of the electric field and aircraft net charge are also quantified in volts per meter and coulombs, respectively.

From Poisson's equation for electrostatics and Ohm's law, $\rho/\varepsilon_0 = (1/r^2)(\mathrm{d}/\mathrm{d}r)(r^2E)$ and $I = sk\rho(r)E(r)$ for corona current I flowing through a shell. (Here, s is the shell's area and k is the ion mobility. For a semisphere, $s = 2\pi r^2$.) Substituting Eqs. (4) and (5) into Poisson's equation and Ohm's law, the corona models of the two wing tips can be established. The computational results are

$$I_{\text{left}} = 2\pi\varepsilon_0 w(828.1Q + 162.1E_y) \times 10^6 - \frac{6.85\pi\varepsilon_0 w^3 \cdot 10^6}{828.1Q + 162.1E_y} \text{ (microamperes)} \tag{6}$$

$$I_{\text{right}} = -\left(2\pi\varepsilon_0 w(-828.1Q + 162.1E_y) \times 10^6 - \frac{6.85\pi\varepsilon_0 w^3 \cdot 10^6}{-828.1Q + 162.1E_y}\right) \text{ (microamperes)} \tag{7}$$

where w is the wind speed (in meters per second) and determines the radius of the outer boundary of the semispherical transition region by $kE(r) = w$. See [13] for more modeling details. For convenience of analysis, the units of the electric field, net charge, and current are quantified in kilovolts per meter, microcoulombs, and microamperes in Eqs. (6) and (7). The rest of this paper follows such an arrangement of units.

Taking the corona breakdown strength as E_m (kilovolts per meter), then

$$|2990Q + 585E_y| = E_m \tag{8}$$

namely, $|E(0,\text{left})| = E_m$, determines the triggering conditions of Q (microcoulombs) and E_y (kilovolts per meter) for a corona of the left wing tip, and

$$|-2990Q + 585E_y| = E_m \tag{9}$$

namely, $|E(0,\text{right})| = E_m$, determines the triggering conditions of Q (microcoulombs) and E_y (kilovolts per meter) for a corona of the right wing tip.

IV. Mill Locations and Calibration Matrix

At least four mills are needed to measure the four unknowns, including three field components and the aircraft net charge. Mill locations are important for reliable measurements [15]. The distribution of mills must cover all the components of the ambient electric fields in the aircraft frame. At the same time, the locations will be better if the mills do not interfere with aircraft systems. The latest calibration methods by Koshak [6] and Koshak and Mach [7] do not require the mills to be symmetrically placed, but this does not mean that the placement is no longer important. As Koshak and Mach emphasized, each mill should be dominated by a different field component. For the purpose of theoretical study, and taking into consideration the aforementioned requirements, a version of the four mills' installation is shown in Fig. 3, in which the arrows indicate the

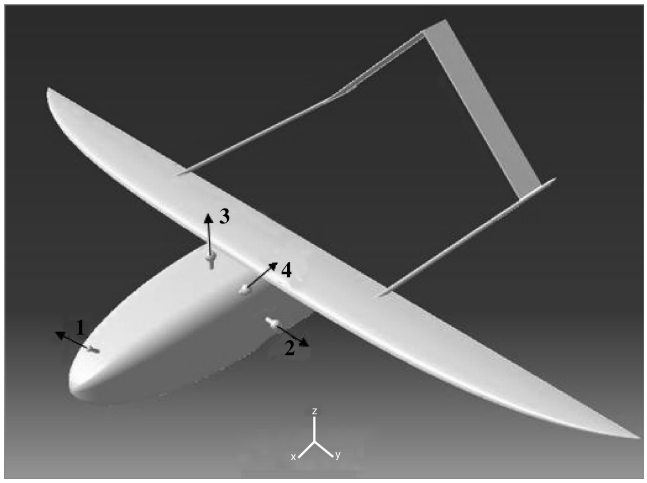

Fig. 3 Proposed mill placements on the TF-1.

mills' orientations. Also considered in this version is the contribution of aircraft net charge to the measurements of the mills. As shown in the wing-tip electric field computational results in Eqs. (2) and (3), the contribution of net charge to the mills' measurements is much greater than that of the electric field components when the mills are close to the surface. To diminish the contribution of net charge, these four mills protrude about 3–5 cm from the surface.

Because no mills have been installed on a TF-1 in reality, the calibration matrix, which determines the input–output relations between the atmospheric electric field, aircraft net charge, and the measurements, cannot be obtained through effective in-flight calibration methods for these four mills. However, it is not so important to obtain an in-flight calibration matrix, as it generally involves some indeterminable errors. At this point of theoretical study, we would rather employ a theoretical method to obtain a more reliable calibration matrix. Also at this point, it is not necessary to be concerned with the performances of any suitable mills. That is, we propose perfect mills without drifts or measurement errors. Thus, the numerical calibration method of Mazur et al. [15] is employed to calibrate the mills.

Assuming insignificant the influences from the small protuberant parts of the mills to the charge distribution on the aircraft surface, the field mills' input–output relationships can be determined by the distorted fields when the field mills are not present. That is, we obtain the calibration relations by computing the electric fields at the points where the mills are placed. For the orientation vector $\boldsymbol{v}_i$ and the distorted field $\boldsymbol{E}_i$ (kilovolts per meter) of mill i, its output m_i (kilovolts per meter) is $m_i = \boldsymbol{v}_i \bullet \boldsymbol{E}_i$. The field $\boldsymbol{E}_i$ can be calculated by the same method used in Sec. II. The computational results are

$$m_1 = 3.99E_x + 0.63E_z + 25.28Q \tag{10}$$

$$m_2 = 0.51E_x + 0.7E_y - 0.56E_z + 8.96Q \tag{11}$$

$$m_3 = 0.91E_x + 1.02E_z + 11.75Q \tag{12}$$

$$m_4 = 0.7E_x + 0.49E_y + 0.6E_z + 8.67Q \tag{13}$$

Here, Q is in microcoulombs. In this placement version, the mill 1 measurement is dominated by E_x, the mill 2 measurement is dominated by E_y, and the mill 3 measurement is dominated by E_z. All the measurements are also dominated by net charge. Transforming Eqs. (10–13) into matrix form, we obtain

$$\begin{bmatrix} E_x \\ E_y \\ E_z \\ Q \end{bmatrix} = \begin{bmatrix} 0.4266 & -0.5876 & -1.0880 & 0.8383 \\ -0.0532 & -0.1955 & -1.4447 & 2.3156 \\ -0.0887 & -0.7654 & -0.0308 & 1.0919 \\ -0.0255 & 0.1118 & 0.1723 & -0.1595 \end{bmatrix} \begin{bmatrix} m_1 \\ m_2 \\ m_3 \\ m_4 \end{bmatrix} \tag{14}$$

V. Wing-Tip Corona Effect on Retrieval of Electric Field

A. Corona Disturbance on Mills

We now derive the theoretical numeric computational method of disturbance on each mill caused by wing-tip corona emissions. Corona ions are swept away by the airstream to form ion plumes, which emanate from the wing tips. The ions are also moved by ambient electric fields, which produce an electrical force on the ions. Hence, the movement of ions consists of two parts: one is the airstream flow, and the other is the velocity produced by the electrical force. For the electric field vector $\boldsymbol{E}$ in the aircraft body frame, ion mobility k, and wind speed w, the ion velocity relative to the aircraft is $\boldsymbol{u} = [-w + kE_x \quad kE_y \quad kE_z]^T$. With the further assumption that $\boldsymbol{E}$ and w are constant throughout the computational time, the plume path can be seen as a line. The disturbances on the mills can be assessed as follows.

The derivation configuration is shown in Fig. 4. We first compute the corona disturbances in the plane formed by the ion plume line and the point where the mill is placed, namely, plane II (see Fig. 4a). Let the ith mill location be $\boldsymbol{r}_i$ and the wing-tip coordinate be $\boldsymbol{r}_{\text{tip}}$. The parameters in Fig. 4b are

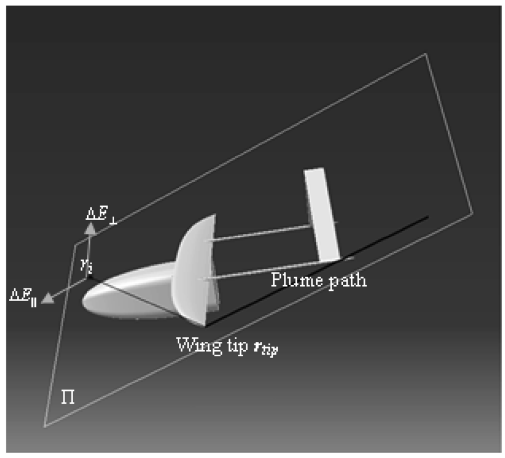

a) 3D sketch map of computational plane

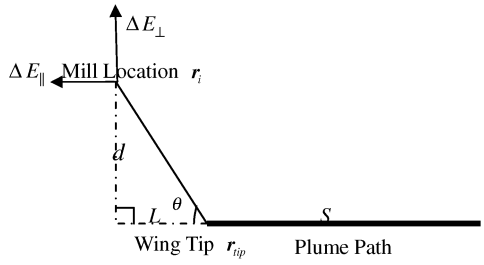

b) Computational plane and variables

Fig. 4 Corona disturbance computational configuration.

$$L = -\frac{(\boldsymbol{r}_i - \boldsymbol{r}_{\text{tip}}) \bullet \boldsymbol{u}}{|\boldsymbol{u}|} \tag{15}$$

$$d = \sqrt{|\boldsymbol{r}_i - \boldsymbol{r}_{\text{tip}}|^2 - L^2} \tag{16}$$

$$S = |\boldsymbol{u}|\Delta t \tag{17}$$

where Δt is the time interval. Taking the reasonable assumption that the corona current is constant in the time interval Δt, the line charge density σ of the ion plume is

$$\sigma = I_c/|\boldsymbol{u}| \tag{18}$$

The disturbance on mill i is decomposed into two parts: one is parallel to the plume path, namely, $\Delta E_{\parallel}$, and the other is perpendicular to the plume path, namely, $\Delta E_{\perp}$. These two parts can be computed by the electric field integral of the plume ions. The integral results are

$$\begin{aligned}\Delta E_{\parallel} &= \int_L^{L+S} \frac{\sigma}{4\pi\varepsilon_0(x^2+d^2)} \frac{x}{\sqrt{(x^2+d^2)}}\,\mathrm{d}x \\ &= \frac{\sigma}{4\pi\varepsilon_0}\left(\frac{1}{\sqrt{L^2+d^2}} - \frac{1}{\sqrt{(L+S)^2+d^2}}\right)\end{aligned} \tag{19}$$

$$\begin{aligned}\Delta E_{\perp} &= \int_L^{L+S} \frac{\sigma}{4\pi\varepsilon_0(x^2+d^2)} \frac{d}{\sqrt{(x^2+d^2)}}\,\mathrm{d}x \\ &= \frac{\sigma}{4\pi\varepsilon_0 d^2}\left(\frac{L+S}{\sqrt{(L+S)^2+d^2}} - \frac{L}{\sqrt{L^2+d^2}}\right)\end{aligned} \tag{20}$$

Substituting these two parts into the forms of vectors in the aircraft body frame yields

$$\Delta \boldsymbol{E}_{\parallel} = -\Delta E_{\parallel} \frac{\boldsymbol{u}}{|u|} \tag{21}$$

$$\Delta \boldsymbol{E}_{\perp} = \Delta E_{\perp} \frac{\boldsymbol{u} \times (\boldsymbol{r}_i - \boldsymbol{r}_{\text{tip}}) \times \boldsymbol{u}}{|\boldsymbol{u} \times (\boldsymbol{r}_i - \boldsymbol{r}_{\text{tip}}) \times \boldsymbol{u}|} \tag{22}$$

Therefore, the total disturbance on measurement m_i of mill i is

$$\Delta m_i = \boldsymbol{v}_i \bullet (\Delta \boldsymbol{E}_{\parallel} + \Delta \boldsymbol{E}_{\perp}) \tag{23}$$

As defined above, $\boldsymbol{v}_i$ is the orientation of mill i.

B. Simplified Disturbance Model

The disturbance computational method still cannot display the aspects of the wing-tip corona effects. Instead, the approximate disturbance model is useful. In this section, we aim to establish such approximate disturbance to visualize the wing-tip corona effects.

Taking a wind speed of 30 m/s as the TF-1's flight speed, the time interval Δt as 1 s, and the ion mobility k as 1.5×10^{-4} $\mathrm{m^2 \cdot s^{-1} \cdot V^{-1}}$ as an average value for ions in air at atmospheric pressure, we computed the disturbances on all mills under different ambient situations. Computational results showed that the disturbance on m_i from the left (and right) wing-tip corona emissions is almost proportional to E_y and Q for constant E_z and E_x. When E_y and Q vary, the disturbance varies in a nonlinear way.

Mill 1: For constant E_z and E_x, the disturbance on mill 1 from the left wing-tip corona emissions can be expressed as a linear form:

$$\Delta m_1^l = aE_y + bQ + c \tag{24}$$

However, the parameters a, b, and c vary with E_z and E_x. We fitted these parameters in a least-squares sense when given different E_z and E_x (see the Appendix). The results are shown in Fig. 5. Data in Fig. 5 show that a, b, and c are not constant with the variation of E_z and E_x components. The surfaces in Fig. 5 indicate that such variation is

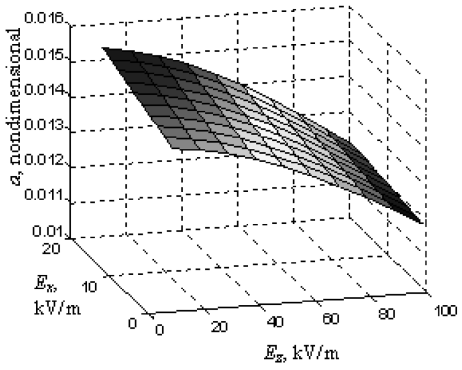

a) Fitted results of *a*

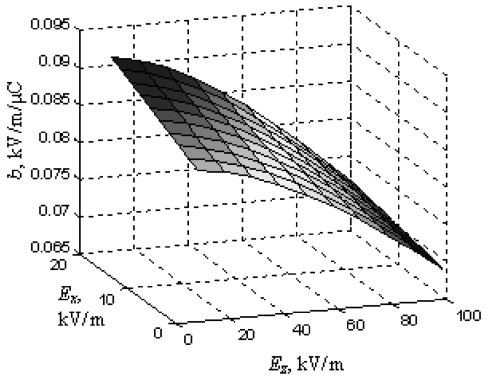

b) Fitted results of *b*

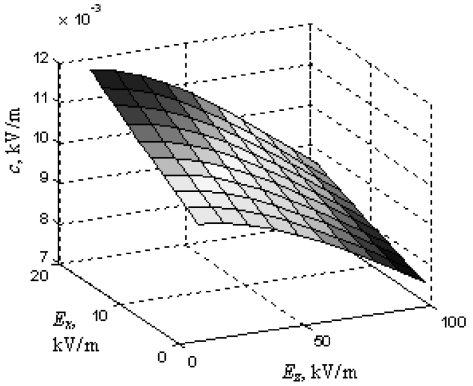

c) Fitted results of *c*

Fig. 5 Fitted *a*, *b*, and *c* to different E_x and E_z.

nonlinear. However, the surfaces in Fig. 5 are rather close to planes. This means that a, b, and c can be seen as proportional to E_z and E_x. For components E_z and E_x, the approximate variations are

$$a = a_1E_x + a_2E_z + a_3 \tag{25}$$

$$b = b_1E_x + b_2E_z + b_3 \tag{26}$$

$$c = c_1E_x + c_2E_z + c_3 \tag{27}$$

Substituting Eqs. (25–27) into Eq. (24), we obtain

$$\begin{aligned}\Delta m_1^l = {} & a_3E_y + b_3Q + c_1E_x + c_2E_z + c_3 \\ & + a_1E_xE_y + a_2E_zE_y + b_1E_xQ + b_2E_zQ\end{aligned} \tag{28}$$

Parameters a_i, b_i, and c_i can also be fitted in a least-squares sense (see the Appendix). The fitted results are

$$a_1 = 0.00005, \qquad a_2 = -0.00014, \qquad a_3 = 0.0269 \tag{29}$$

$$b_1 = 0.0003, \qquad b_2 = -0.00075, \qquad b_3 = 0.1412 \tag{30}$$

$$c_1 = 0.00002, \qquad c_2 = -0.00002, \qquad c_3 = 0.0031 \tag{31}$$

The mean square error of the fitting result is only $9.4e-5$, which indicates that the simplified model of Eq. (28) is precise. Equation (28) contains two parts: the linear effects, namely, a_3E_y, b_3Q, c_1E_x, c_2E_z, and c_3, and the nonlinear coupling effects, namely, $a_1E_xE_y$, $a_2E_zE_y$, b_1E_xQ, and b_2E_zQ.

Previous field observations in clouds show that E_x and E_y components can run up to 20 kV/m, but rarely exceed 20 kV/m (influenced by the position and attitude of the aircraft); the E_z component is always stronger than these two components, which can run up to hundreds of kilovolts per meter. However, according to Winn and Moore [16] and Winn and Schwede [17], field strength rarely exceeds 100 kV/m. They observed fields stronger than 100 kV/m only seven times in 90 observations. Thus, we can ignore some small parts, such as c_1E_x, c_2E_z, c_3, E_xE_y, and E_xQ (these terms remain small in most regions), in Eq. (28). Because the E_z component is much stronger, the effects caused by the nonlinear parts, namely, E_zE_y and E_zQ, remain. Thus, the disturbance on mill 1 from the left wing-tip corona can be simplified as

$$\Delta m_1^l = 0.0269E_y + 0.1412Q - 0.00014E_zE_y - 0.00075E_zQ \tag{32}$$

The simplified disturbance does not contain the E_x component. This can be explained as follows: E_x is generally smaller than 20 kV/m when penetrating clouds. Taking ion mobility k as 1.5×10^{-4} $m^2 \cdot s^{-1} \cdot V^{-1}$, the ion velocity due to E_x is no more than 3 m/s. This value is much smaller than the airstream speed of 30 m/s. Hence, the relative ion speed $\boldsymbol{u}$ is $\boldsymbol{u} = [-w \quad kE_y \quad kE_z]^T$, and the effect of E_x is ignored.

Other mills: In a similar fashion, we can establish the same models for the other mills. Ignoring the small parts as for Δm_1^l, the numerical results are

$$\Delta m_2^l = -0.033E_y - 0.1593Q + 0.00005E_zE_y + 0.00024E_zQ \tag{33}$$

$$\Delta m_3^l = 0.0022Q - 0.00016E_zE_y - 0.0009E_zQ \tag{34}$$

$$\Delta m_4^l = -0.022E_y - 0.104Q - 0.0001E_zE_y - 0.0006E_zQ \tag{35}$$

$$\Delta m_1^r = -0.037E_y + 0.1934Q + 0.0001E_zE_y - 0.0003E_zQ \tag{36}$$

$$\Delta m_2^r = -0.016E_y + 0.089Q - 0.0001E_zQ \tag{37}$$

$$\Delta m_3^r = 0.002Q + 0.00018E_zE_y - 0.0006E_zQ \tag{38}$$

$$\Delta m_4^r = -0.011E_y + 0.061Q + 0.0001E_zE_y - 0.0003E_zQ \tag{39}$$

The superscripts l and r denote the effect of the left and right wing-tip corona emissions, respectively. The unit of disturbance is kilovolts per meter.

Note that the corona trigger conditions for the left and right wing-tip corona emissions, namely, Eqs. (8) and (9), are different. That is, Δm_i^l exists only when $|2990Q + 585E_y| \geq E_m$, whereas Δm_i^r exists when $|-2990Q + 585E_y| \geq E_m$. Therefore, the total disturbance on any mill is not the summation of Δm^r and Δm^l for all situations. When corona emissions take place at both wing tips, the total disturbance is given by the summation of Δm^r and Δm^l:

$$\Delta m_1 = -0.0101E_y + 0.33Q - 0.00004E_zE_y - 0.0011E_zQ \tag{40}$$

$$\Delta m_2 = -0.049E_y - 0.07Q + 0.00005E_zE_y + 0.00014E_zQ \tag{41}$$

$$\Delta m_3 = 0.0042Q + 0.00002E_zE_y - 0.0015E_zQ \tag{42}$$

$$\Delta m_4 = -0.033E_y - 0.043Q - 0.0009E_zQ \tag{43}$$

C. Quantitative Analysis of Corona Effect

In the previous section, we presented the nonlinear effect of wing-tip corona emissions, which mainly contains E_zE_y and E_zQ. The small fitted parameters in Eq. (28) indicate that the nonlinear effect caused by corona emissions is significant only when the ambient field is strong and the net charge on the aircraft surface is high. If the ambient field is weak, the corona effect can be seen as linear.

Consider such a region, where $E_z = 100$ kV/m, $E_y = 10$ kV/m, and $E_x = 10$ kV/m. Assume the net charge on the TF-1 is -10 μC (which could be a conservative value). If the corona breakdown strength is 2600 kV/m, then both wing tips will emit corona ions in such a situation, according to the breakdown equations, Eqs. (8) and (9). We computed the linear effect (the summation of the two terms E_y and Q) and the nonlinear effect (the summation of the two terms E_zE_y and E_zQ) for all four mills, according to Eqs. (40–43). The computational results are tabulated in Table 1, in which the unit of the disturbance is kilovolts per meter. The data in Table 1 clearly show that almost all the disturbances of linear parts are larger than the nonlinear parts (an exception is mill 3, for which the linear parts are almost zeros, whereas its nonlinear parts are close to 1 kV/m.). Nevertheless, the nonlinear parts, which could be half of the corresponding linear parts, are still significant. For example, for mills 1 and 4, the nonlinear disturbances exceed half of their linear parts. These nonlinear effects are too significant to be ignored.

In addition, in such a situation, substituting Eqs. (40–43) into Eq. (28), the errors in retrieving field components and net charge are

$$\Delta E_x = -0.0032E_y + 0.1413Q - 0.00007E_zE_y + 0.00033E_zQ \tag{44}$$

$$\Delta E_y = -0.0663E_y - 0.1095Q - 0.00004E_zE_y + 0.00011E_zQ \tag{45}$$

$$\Delta E_z = 0.00237E_y - 0.02278Q - 0.00004E_zE_y - 0.00095E_zQ \tag{46}$$

$$\Delta Q = 0.00004E_y - 0.0087Q + 0.00001E_zE_y - 0.00007E_zQ \tag{47}$$

Substituting the numbers of E_z, E_y, E_z, and Q into these equations, the retrieval errors for electric field and net charge are $\Delta E_x = -1.88$ kV/m, $\Delta E_y = 0.29$ kV/m, $\Delta E_z = 1.98$ kV/m, and $\Delta Q = 0.178$ μC, respectively. The relative errors are 18.8, 2.9, 2, and 1.78%, respectively. If we drop the nonlinear effect in Eqs. (44–47), we yield $\Delta E_x = -1.45$ kV/m, $\Delta E_y = 0.43$ kV/m, $\Delta E_z = 0.25$ kV/m, and $\Delta Q = 0.087$ μC, respectively. Comparing these two sets of numbers, it is evident that the influence of dropping the nonlinear effect is somewhat significant, especially for the last three errors, namely, ΔE_y, ΔE_z, and ΔQ. Because the relative errors

Table 1 Linear and nonlinear corona effect on mills, where $E_z = 100$ kV/m, $E_y = 10$ kV/m, $E_x = 10$ kV/m, and $Q = -10$ μC

	Δm_1^l	Δm_2^l	Δm_3^l	Δm_4^l	Δm_1^r	Δm_2^r	Δm_3^r	Δm_4^r
Nonlinear	0.61	−0.19	0.74	0.5	0.4	0.1	0.78	0.4
Linear	−1.14	1.26	−0.02	0.82	−2.3	−1.05	−0.02	−0.72

of these three terms are small, this influence could be ignored. However, there is a significant absolute disagreement for ΔE_x, which is 0.43 kV/m. For precise measurement of E_x, the nonlinear effect could not be dropped.

Previous studies have shown that the retrieval of the E_x field component has been problematic. The early T-28 aircraft placed a mill oriented to the x axis at the fuselage tail. Research has indicated that measurement of this mill is heavily affected by the tail corona emissions that pass directly by it. Our earlier numeric computational results also show that the retrieval of E_x is most likely to be affected by corona emissions. Yet, even more notable is that, in our version of installation, all the mills are somewhat far from the wing-tip corona emissions, and no corona ions pass by them. Visualizing a manned aircraft with a more complex surface than that of the TF-1, corona emissions can occur at more locations than the two wing tips. There would be many more corona points with a larger magnitude of corona currents due to the complex surface and bigger net charge Q of the manned aircraft. This aspect of larger manned aircraft makes it more important to highlight not only the tail corona effect but also other remote-corona-point effects for precise and reliable measurements. Also important is that the nonlinear corona effects, especially the term of E_zQ, would be greater for a larger Q (maybe hundreds of microcoulombs). The error caused by dropping the nonlinear effect for E_x would be much greater. Thus, the nonlinear effect cannot be ignored for manned aircraft.

VI. Conclusions

We conducted a theoretical study of the effects of wing-tip corona emissions to understand how electric field measurements are affected. It is commonly recognized that the mills' measurements are nonlinear to the ambient field components and net charge when corona takes place. Owing to the difficulties in modeling processes such as corona emission, previous studies did not consider the nonlinear effects. The theoretical studies in this paper present two further findings relevant to the nonlinear corona effects:

1) The wing-tip corona effects on field measurements are nonlinear and can be decomposed into two parts: one is mainly linear with E_y and Q, and another is mainly linear with E_zE_y.

2) The retrieval of E_x is most problematic whether or not mills are located downstream of corona plumes. For manned aircraft, the nonlinear effect could not be ignored.

The numerical data in this paper were obtained from only two corona points. Because a manned aircraft has a more complex surface and can charge more on its surface, the corona effect should be greater than the numerical results discussed in this paper. To obtain precise field measurements, it is necessary to relieve corona effects not only for fuselage tail corona emissions, but also for other possible corona emissions. Arriving at a solution for corona effects may involve corona discharge predictions as well as corona magnitude estimations, which would be extremely intricate processes.

Appendix: Least-Squares Estimation for the Corona Effect Model

Repeating Eq. (24), a least-squares solution for a, b, and c can be obtained as follows.

Let E_x and E_z be specified and E_y and Q be variables. For a set of discrete numbers of E_y and Q, the corresponding discrete number of Δm_1^l can be calculated by Eq. (22) in Sec. V.A with specified E_x and E_y. Hence, we obtain

$$\Delta m_1^l(i) = aE_y(i) + bQ(i) + c \quad \text{(for special } E_x \text{ and } E_y\text{)} \tag{A1}$$

where i is the index. A least-squares solution of a, b, and c is defined as the numbers that minimize

$$\sum (\Delta m_1^l(i) - aE_y(i) - bQ(i) - c)^2$$

Such numbers satisfy

$$\frac{\partial}{\partial a} \sum (\Delta m_1^l(i) - aE_y(i) - bQ(i) - c)^2 = 0 \tag{A2}$$

$$\frac{\partial}{\partial b} \sum (\Delta m_1^l(i) - aE_y(i) - bQ(i) - c)^2 = 0 \tag{A3}$$

$$\frac{\partial}{\partial c} \sum (\Delta m_1^l(i) - aE_y(i) - bQ(i) - c)^2 = 0 \tag{A4}$$

Solving these equations yields

$$\begin{pmatrix} a \\ b \\ c \end{pmatrix} = \begin{pmatrix} \sum E_y^2(i) & \sum E_y(i)Q(i) & \sum E_y(i) \\ \sum E_y(i)Q(i) & \sum Q^2(i) & \sum Q(i) \\ \sum E_y(i) & \sum Q(i) & 1 \end{pmatrix}^{-1} \times \begin{pmatrix} \sum \Delta m_1^l(i)E_y(i) \\ \sum \Delta m_1^l(i)Q(i) \\ \sum \Delta m_1^l(i) \end{pmatrix} \tag{A5}$$

Given a different set of E_x and E_y, parameters a, b, and c in Eq. (25) can be calculated once again.

The parameters in Eq. (28) can be solved in the same fashion. Because there are nine unknowns in Eq. (28), the derivation is lengthy. However, the least-squares theory is the same as the one given here.

References

[1] Mo, Q., Feind, R. E., Kopp, F. J., and Detwiler, A. G., "Improved Electric Field Measurements with the T-28 Armored Research Airplane," *Journal of Geophysical Research*, Vol. 104, No. D20, 1999, pp. 24,485–24,497. doi:10.1029/1999JD900834

[2] Jones, J. J., "Electric Charge Acquired by Airplanes Penetrating Thunderstorms," *Journal of Geophysical Research*, Vol. 95, No. D10, 1990, pp. 16,589–16,600. doi:10.1029/JD095iD10p16589

[3] Jones, J. J., Winn, W. P., and Han, F., "Electric Field Measurements with an Airplane: Problems Caused By Emitted Charge," *Journal of Geophysical Research*, Vol. 98, No. D3, pp. 5,235–5,244. doi:10.1029/92JD02686

[4] Blackslee, R. J., Mach, D., Desch, M., Goldberg, R. A., Farrell, W. M., and Houser, J. G., "The Altus Cumulus Electrification Study (ACES): A UAV-Based Science Demonstration," AIAA Paper 2002-3405, 2002.

[5] Koshak, W. J., Bailey, J., Christian, H. J., and Mach, D. M., "Aircraft Electric Field Measurements: Calibration and Ambient Field Retrieval," *Journal of Geophysical Research*, Vol. 99, No. D11, 1994, pp. 22,781–22,792. doi:10.1029/94JD01682

[6] Koshak, W. J., "Retrieving Storm Electric Fields from Aircraft Field Mill Data. Part I: Theory," *Journal of Atmospheric and Oceanic Technology*, Vol. 23, No. 10, 2006, pp. 1,289–1,302. doi:10.1175/JTECH1917.1

[7] Koshak, W. J., Mach, D. M., Christian, H. J., Stewart, M. F., and Bateman, M. G., "Retrieving Storm Electric Fields from Aircraft Field Mill Data. Part II: Applications," *Journal of Atmospheric and Oceanic Technology*, Vol. 23, No. 10, 2006, pp. 1,303–1,322. doi:10.1175/JTECH1918.1

[8] Bateman, B. G., Stewart, M. F., Blakeslee, R. J., Daskar, D, Podgorny, S. J., Christian, H. J., and Mach, D. M., "A Low-Noise, Microprocessor-Controlled, Internally Digitizing Rotating-Vane Electric Field Mill for Airborne Platforms," *Journal of Atmospheric and Oceanic Technology*, Vol. 24, No. 7, 2007, pp. 1,245–1,255. doi:10.1175/JTECH2039.1

[9] Winn, W. P., "Aircraft Measurement of Electric Field: Self-Calibration," *Journal of Geophysical Research*, Vol. 98, No. D4, 1993, pp. 7,351–7,356. doi:10.1029/93JD00165

[10] Mach, D. M., and Koshak, W. J., "General Matrix Inversion Technique for the Calibration of Electric Field Mill Arrays on Aircraft Platforms," *Journal of Atmospheric and Oceanic Technology*, Vol. 24, No. 9, 2007, pp. 1,576–1,587.

doi:10.1175/JTECH2080.1

[11] Da, X., Hong, L., and Shen, H., "Computation Model of Electric Field for Aircraft Penetrating Clouds," *2008 Asia Simulation Conference—7th international Conference on System Simulation and Scientific Computing*, Inst. of Electrical and Electronics Engineers, New York, 2008, pp. 721–725.
doi:10.1109/ASC-ICSC.2008.4675454

[12] Da, X., Shen, H., and Hong, L., "New Electric Field Computation Method for Aircraft," *Journal of Aircraft*, Vol. 46, No. 2, 2009, pp. 557–561.
doi:10.2514/1.38699

[13] Da, X., Shen, H., and Hong, L., "Magnitude of Corona Current Caused by Aircraft Net Charge," *Journal of Aircraft* (to be published).

[14] Chapman, S., "The Magnitude of Corona Point Discharge Current," *Journal of the Atmospheric Sciences*, Vol. 34, No. 11, 1977, November, pp. 1,801–1,809.
doi:10.1175/1520-0469(1977)034<1801:TMOCPD>2.0.CO;2

[15] Mazur, V., Ruhnke, L. H., and Rudolph, T., "Effect of *E*-Field Location on Accuracy of Electric Field Measurements with Instrumented Airplane," *Journal of Geophysical Research*, Vol. 92, No. D10, 1987, pp. 12,013–12,019.
doi:10.1029/JD092iD10p12013

[16] Winn, W. P., and Moore, C. B., "Electric Field Measurements in Thunderclouds Using Instrumented Rockets," *Journal of Geophysical Research*, Vol. 76, No. 21, 1971, pp. 5003–5017.
doi:10.1029/JC076i021p05003

[17] Winn, W. P., Schwede, G. W., and Moore, C. B., "Measurements of Electric Fields in Thunderclouds," *Journal of Geophysical Research*, Vol. 79, No. 12, 1974, pp. 1761–1767.
doi:10.1029/JC079i012p01761